

# Ring Puckering: A Metric for Evaluating the Accuracy of AM1, PM3, PM3CARB-1, and SCC-DFTB Carbohydrate QM/MM Simulations

Christopher B. Barnett and Kevin J. Naidoo\*

Scientific Computing Research Unit and Department of Chemistry, University of Cape Town,  
Rondebosch 7701, South Africa

Received: August 12, 2010; Revised Manuscript Received: October 30, 2010

The puckered conformations of furanose and pyranose carbohydrate rings are central to analyzing the action of enzymes on carbohydrates. Enzyme reaction mechanisms are generally inaccessible to experiments and so have become the focus of QM(semiempirical)/MM simulations. We show that the complete free energy of puckering is required to evaluate the accuracy of semiempirical methods used to study reactions involving carbohydrates. Interestingly, we find that reducing the free energy space to lower dimensions results in near meaningless minimum energy pathways. We analyze the furanose and pyranose free energy pucker surfaces and volumes using AM1, PM3, PM3CARB-1, and SCC-DFTB. A comparison with DFT optimized structures and a HF free energy surface reveals that SCC-DFTB provides the best semiempirical description of five- and six-membered carbohydrate ring deformation.

## 1. Introduction

Carbohydrate monomers are conformationally very complex. The complexity stems from the possibility of multiple linkages that can be formed via the numerous hydroxyl groups decorating the periphery of the flexible monosaccharide rings and the wide range of pucker conformers available to these five-membered (furanose) and six-membered (pyranose) rings. This conformational diversity of the basic monomers used to construct oligosaccharides and biopolymers is most likely the reason for the extensive presence of carbohydrates in nature and the diverse range of functions they perform. In cellular systems, saccharides are a primary source for fuel, they act as metabolic intermediates in cellular formative pathways, and are key structural units in the genetic (RNA/DNA) framework.

The nature of furanose and pyranose ring conformational pucker is critical in the formation of transition states found along the reaction paths catalyzed by phosphorylases,<sup>1</sup> ribosyl transferases, hydrolases,<sup>2</sup> and dehalogenases.<sup>3</sup> Pyranose rings play a prominent role in carbohydrate processing enzymes, including glycosidases (the enzymes responsible for the breakdown of di-, oligo-, and polysaccharides,) and glycosyltransferases (the enzymes which transfer saccharides to other saccharide moieties). Glycoside chemistry is largely the chemistry of the oxocarbenium ion formed in the transition state (TS); the conformers that meet this criteria for this are shown in Figure 1.

In the case of five-membered rings, an example of the importance of ring conformations is in the base excision repair (BER) enzymes. These enzymes remove nucleobases from DNA in the first step of the repair of many types of DNA damage.<sup>4</sup> The mechanisms of *N*-glycoside hydrolysis and *N*-glycosyl transfer reactions have similarities to the *O*-glycoside (polysaccharide) hydrolyses. As in the pyranose case, there is an accumulation of positive charge on the sugar ring at the TS. Hyperconjugation stabilizes the carbocation when the dihedral angle between the C2'-H2' bond and the developing empty p-orbital on C1' is at 0° or 180°.<sup>5</sup> The hyperconjugation in

furanose oxocarbenium ions therefore significantly depends on the ring pucker conformation. When a strong π-bond develops between C1' and the ring oxygen, O4', one of two envelope conformations, 3'-endo or 3'-exo (Figure 2) could form.<sup>4</sup>

The investigation of reactions in carbohydrate processing enzymes via experiments has limited possibilities. While the mechanism can be probed with (i) repeated X-ray structural analysis of mutated enzymes or enzymes bound to inhibitors<sup>6,7</sup> and (ii) kinetic isotope effect (KIE) experiments,<sup>8</sup> the nature of the TS remains inaccessible to experimentalists. Therefore, the use of computational methods, particularly hybrid quantum classical (QM/MM) ones, has become central to the investigation of enzyme reaction mechanisms and the conformational and electronic nature of the TS.

Herein lies the problem when simulating carbohydrates. Unless the semiempirical methods used in QM/MM simulations are able to model the intricate conformational and electronic transitions of furanose and pyranose monosaccharides accurately, the mechanistic details and TS structures derived from these simulations may be meaningless. We address this matter here by calculating the complete free energy of pucker surfaces for ribose and the free energy of pucker volumes for glucose monosaccharides using AM1,<sup>9</sup> PM3,<sup>10</sup> PM3CARB-1,<sup>11</sup> and SCC-DFTB<sup>12</sup> semiempirical methods. We then compare them with each other, to selected DFT RB3LYP/6-311++G(d,p) stationary structures, and to a free energy 6-31G Hartree–Fock surface.

## 2. Pucker Definitions

Five-membered rings can be classified into envelopes (E) and twists (T), and similarly six-membered rings can be classified into chairs (C), boats (B), skew (S), the form between two boats, envelopes (E), and half-boats (H).<sup>13</sup> The mathematical definition of these conformers was based on a spherical polar coordinate system which was introduced by Cremer and Pople in their classic 1975 publication.<sup>14</sup> These definitions proved very popular despite the cumbersome relationship between these coordinates and physically meaningful stresses and strains on the rings. More

\* To whom correspondence should be addressed. E-mail: Kevin.Naidoo@uct.ac.za. Fax: +27-21-686-4333.

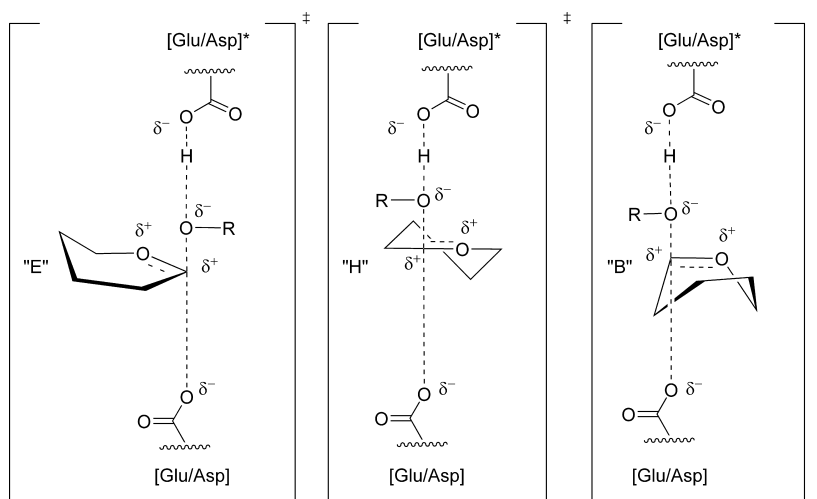


**Figure 1.** Possible oxocarbenium pyranose transition states that may occur in acid-catalyzed processes. The anomeric carbon, which has planar character, may only exist in envelope (E), half-chair (H), or boat (B) conformers as represented by figures on the left, center, and right, respectively. The specific conformers that can be accessed are  $^4\text{H}_3$ ,  $^3\text{H}_4$ ,  $^4\text{H}_5$ ,  $^5\text{H}_4$ ,  $^2\text{H}_3$ ,  $^3\text{H}_2$ ,  $^4\text{E}, \text{E}_4$ ,  $^3\text{E}, \text{E}_3$ , and  $^{2,5}\text{B}, \text{B}_{2,5}$ . \* indicates that the amino acid is protonated.

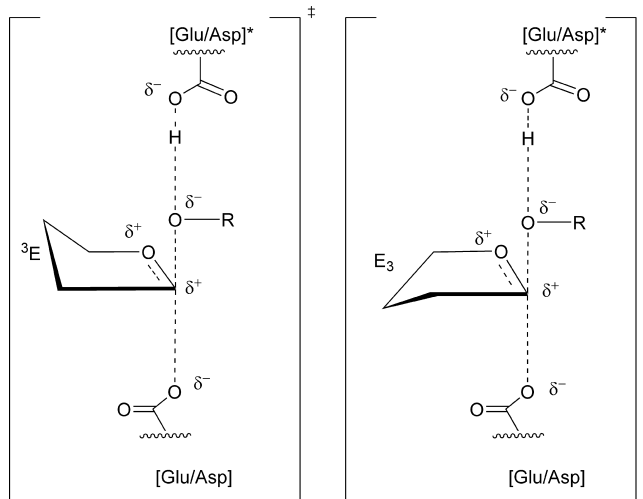


**Figure 2.** Possible oxocarbenium furanose transition states that may occur in acid-catalyzed processes. The anomeric carbon, which has planar character, may only exist as the  $^3\text{E}$  (also known as 3-endo) or  $\text{E}_3$  (3-exo) conformers. \* indicates that the amino acid is protonated.

recently, Hill and Reilly proposed a triangular decomposition coordinate set that enables a ready description of ring conformers as a function of triangular planes deviating from a reference plane placed on the monosaccharide ring.<sup>15</sup>

While other descriptions of ring puckering have been proposed<sup>16</sup> and are in popular use,<sup>14</sup> we found the triangular decomposition<sup>15</sup> to be particularly amenable to the free energy from adaptive reaction coordinate forces (FEARCF) method.<sup>17</sup> Furthermore, the decomposition of a monocyclic ring into a reference plane and rotatable (puckering) planes translates into an easily understood physical description.<sup>15,18,19</sup> For an  $N$ -membered ring there are  $N - 2$  planes; a central reference plane and  $N - 3$  rotatable puckering planes, where the puckering coordinates are the angles between each of the rotatable planes with respect to the central plane. For example, a six-membered ring has a central plane and three puckering planes such that there are three puckering coordinates  $\theta_0, \theta_1, \theta_2 \in [-90^\circ, 90^\circ]$ . The angle of puckering is calculated from

$$\theta_i = \pi/2 - \cos^{-1}[(\mathbf{q}_i \cdot \mathbf{n}) \cdot (||\mathbf{q}_i|| \cdot ||\mathbf{n}||)^{-1}] \quad (1)$$

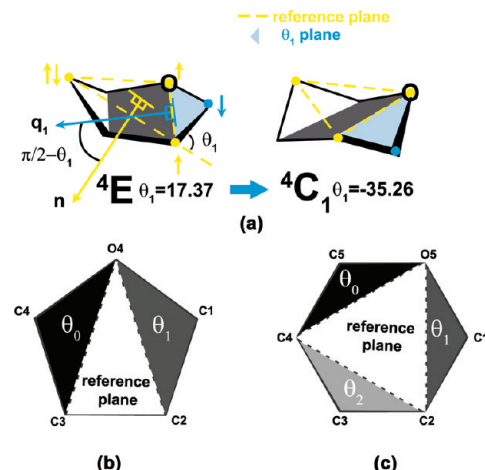
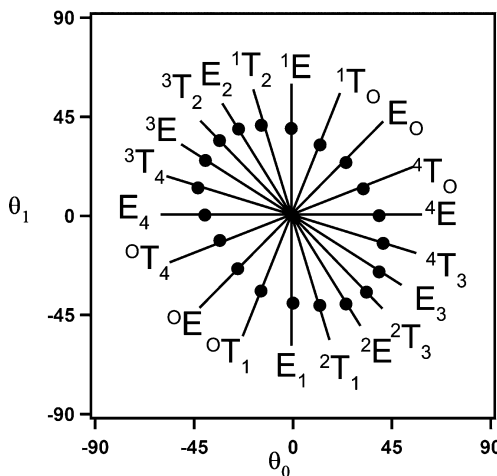


**Figure 3.** (a) FEARCF forces (short arrows) originating from a rotatable plane (blue) using triangular decomposition coordinates for glucose showing a transition from  $^4\text{E}$  conformation to the  $^4\text{C}_1$  conformation. The reference plane and rotatable planes are labeled for (b)  $\beta$ -D-ribose (c) and  $\beta$ -D-glucose.

where  $\mathbf{q}_i$  is a vector normal to the rotatable plane  $i$  and the axis about which the plane rotates, while  $\mathbf{n}$  is the vector normal to the reference plane (shown in Figure 3a for pyranose). These coordinates are illustrated for ribose and glucose in Figure 3, b and c respectively. The reference plane used in the triangular decomposition<sup>15</sup> is not the same as the mean plane used in the Cremer-Pople<sup>14</sup> definition or that of the IUPAC nomenclature for carbohydrate rings. Nonetheless, as with Cremer-Pople coordinates, these puckering coordinates can be mapped to the IUPAC canonical conformers.<sup>15</sup> We show this mapping for furanose in Scheme 1, along with a list of the full set of puckering coordinate values in Table 1. In Scheme 2, we show the canonical conformers for pyranose along with a list of the full set of puckering coordinate values in Table 2. The exact mapping of the Hill-Reilly-proposed puckering coordinates to canonical conformers does depend on the ordering of atoms used to define the reference and puckering planes. They chose C1-C3-C5 in their definition, with C2 as the apex of the puckering plane (or ring flap) defining  $\theta_0$ , C3 as the apex of  $\theta_1$ , and O5 as the apex of  $\theta_2$ . This nomenclature was followed in our earlier work for glucose<sup>19</sup> and similarly for ribose.<sup>18</sup> However, the definitions used in this work are not the same as those previously, since

**SCHEME 1:** Triangular Decomposition Pucker Space for Five-Membered Rings<sup>a</sup>



<sup>a</sup> The origin represents a planar ring. The bold nodes represent the optimized IUPAC conformations of cyclopentane. The line segments branching from the origin represent a range of points at which a specific IUPAC conformation exists. There are 10 envelope, 10 twists, and 1 planar conformer.

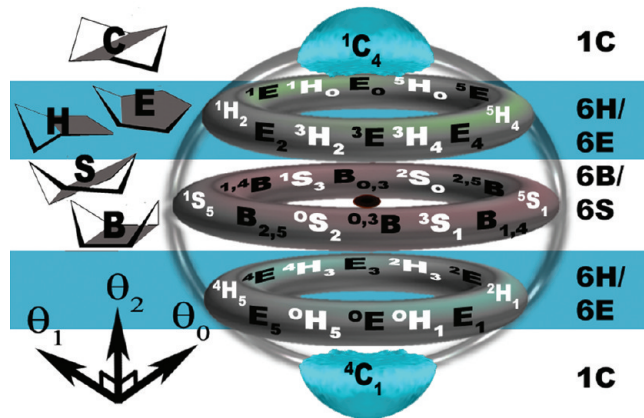
**TABLE 1:** Triangular Decomposition Pucker Coordinates (in deg) That Correspond to Ideal IUPAC Conformers for a Furanose Ring (Based on Cyclopentane)

canonical conformation	$\theta_0$	$\theta_1$
<sup>0</sup> T <sub>1</sub>	-13.10	-33.89
<sup>3</sup> T <sub>4</sub>	-42.16	13.21
<sup>2</sup> T <sub>3</sub>	34.50	-34.50
<sup>1</sup> T <sub>2</sub>	-13.21	42.16
<sup>4</sup> T <sub>0</sub>	33.89	13.11
<sup>1</sup> T <sub>0</sub>	13.10	33.89
<sup>4</sup> T <sub>3</sub>	42.16	-13.21
<sup>3</sup> T <sub>2</sub>	-34.50	34.50
<sup>2</sup> T <sub>1</sub>	13.21	-42.16
<sup>0</sup> T <sub>4</sub>	-33.89	-13.11
E <sub>2</sub>	-24.88	40.00
E <sub>1</sub>	0.00	-39.90
E <sub>0</sub>	24.50	24.50
E <sub>4</sub>	-39.50	0.00
E <sub>3</sub>	39.50	-24.90
<sup>2</sup> E	24.88	-40.00
<sup>1</sup> E	0.00	39.90
<sup>0</sup> E	-24.50	-24.50
<sup>4</sup> E	39.50	0.00
<sup>3</sup> E	-39.50	24.90
P	0.00	0.00

we intend to present free energy surfaces that can be analyzed as a function of the motion of the anomeric carbon and the ring carbon bearing the primary alcohol substituent. This information is necessary for understanding the relationship between the ring pucker and the oxocarbenium ion formation in the transition states of glycosidases.

The reference plane for the furanose ring was chosen as C3—O4—C2 and the two ring flaps were defined as C3—C4—O4 ( $\theta_0$ ) and O4—C1—C2 ( $\theta_1$ ) as shown in Figure 3b. Here,  $\theta_0$  describes the movement of the ring carbon bearing the primary alcohol, while  $\theta_1$  describes the movement of the anomeric carbon into and out of the reference plane. For the pyranose ring the atoms C4—O5—C2 were chosen as the reference plane (Figure 3c) and the three flaps were defined as C4—C5—O5 ( $\theta_0$ ), O5—C1—C2 ( $\theta_1$ ), and C2—C3—C4 ( $\theta_2$ );  $\theta_0$  describes the movement of the carbon to which the primary alcohol moiety (C5) is attached,  $\theta_1$  describes the movement of the anomeric

**SCHEME 2:** Triangular Decomposition Pucker Volume Accessible to Six-Membered Rings Showing the Positions of IUPAC-Labeled Conformers<sup>a</sup>



<sup>a</sup> The origin represents a planar six-membered ring; the axes drawn are with respect to the origin. The “poles” are chair conformers, the “tropics” are half-chair and envelopes, and the “equator” has boat (sofa) and twist-boat (skew-boat) conformers.

**TABLE 2:** Triangular Decomposition Pucker Coordinates (in deg) for the C4—O5—C2 Reference Plane for a Pyranose Ring That Corresponds to IUPAC Canonical Conformers

canonical conformation	$\theta_0$	$\theta_1$	$\theta_2$
B <sub>2,5</sub>	-74.20	35.26	35.26
<sup>1</sup> S <sub>5</sub>	-50.84	50.84	0.00
<sup>0</sup> S <sub>2</sub>	-50.84	0.00	50.84
E <sub>5</sub>	-46.86	0.00	0.00
<sup>4</sup> H <sub>5</sub>	-42.16	9.07	-17.83
<sup>0</sup> H <sub>5</sub>	-42.16	-17.83	9.06
<sup>1,4</sup> B	-35.26	74.2	-35.26
<sup>0,3</sup> B	-35.26	-35.26	74.2
<sup>4</sup> C <sub>1</sub>	-35.26	-35.26	-35.26
<sup>4</sup> E	-35.26	17.37	-35.26
<sup>0</sup> E	-35.26	-35.26	17.37
<sup>4</sup> H <sub>3</sub>	-17.83	9.07	-42.16
<sup>0</sup> H <sub>1</sub>	-17.83	-42.16	9.07
E <sub>2</sub>	-17.37	35.26	35.26
<sup>1</sup> H <sub>2</sub>	-9.07	42.16	17.83
<sup>3</sup> H <sub>2</sub>	-9.07	17.83	42.16
<sup>1</sup> E	0.00	46.86	0.00
<sup>1</sup> S <sub>3</sub>	0.00	50.84	-50.84
<sup>3</sup> E	0.00	0.00	46.86
<sup>3</sup> S <sub>1</sub>	0.00	-50.84	50.84
E <sub>1</sub>	0.00	-46.86	0.00
E <sub>3</sub>	0.00	0.00	-46.86
<sup>2</sup> H <sub>1</sub>	9.07	-42.16	-17.83
<sup>2</sup> H <sub>3</sub>	9.07	-17.83	-42.16
<sup>2</sup> E	17.37	-35.26	-35.26
<sup>1</sup> H <sub>0</sub>	17.83	42.16	-9.07
<sup>3</sup> H <sub>4</sub>	17.83	-9.07	42.16
<sup>1</sup> C <sub>4</sub>	35.26	35.26	35.26
B <sub>1,4</sub>	35.26	-74.20	35.26
B <sub>0,3</sub>	35.26	35.26	-74.2
E <sub>4</sub>	35.26	-17.37	35.26
E <sub>0</sub>	35.26	35.26	-17.37
<sup>5</sup> H <sub>4</sub>	42.16	-9.07	17.83
<sup>5</sup> H <sub>0</sub>	42.16	17.83	-9.06
<sup>5</sup> E	46.86	0.00	0.00
<sup>2</sup> S <sub>0</sub>	50.84	0.00	-50.84
<sup>5</sup> S <sub>1</sub>	50.84	-50.84	0.00
<sup>2,5</sup> B	74.20	-35.26	-35.26

carbon (C1), and  $\theta_2$  describes the movement of a carbon (C3) to which a secondary alcohol is attached.

### 3. Computational Methods

Using the FEARCF method and the Hill–Reilly<sup>15</sup> definition, we calculated the free energy of puckering surface for  $\beta$ -D-ribose and volume for  $\beta$ -D-glucose rings *in vacuo*.

**3.1. Calculation of the Free Energy of Ring Pucker.** The reaction coordinate ( $\xi$ ) for ribose is  $\xi_{\text{ribose}} = (\theta_0, \theta_1)$  while for glucose it is  $\xi_{\text{glucose}} = (\theta_0, \theta_1, \theta_2)$ . The potential of mean force (PMF),  $W(\xi)$  is then calculated as a function of the ( $N - 3$ )-dimensional coordinate set  $\xi$  (where  $N$  is the number of atoms in the ring) and is related to the probability density,  $P(\xi)$  by

$$W(\xi) = -k_B T \ln P(\xi) \quad (2)$$

where  $k_B$  is the Boltzmann constant and  $T$  is the temperature in kelvin. The PMF is derived in a canonical ensemble (constant NVT) giving the Helmholtz free energy. In the FEARCF method, barrier heights separating conformational minima are traversed by applying an adaptive biasing force  $F(\xi)$ . We derive  $F(\xi)$  from the reaction coordinate potential energy  $U(\xi)$  defined from the histogram of previously sampled regions of reaction coordinate space.

$$U(\xi) = k_B T \ln P(\xi) \quad (3)$$

An indication that the sampled surface has converged is when  $U(\xi)$  is equal to the inverse of the free energy function (i.e.,  $U(\xi) = -W(\xi)$ ). Therefore, when applying biased forces from the converged surface in a simulation, the resulting sampling from a long simulation of reaction coordinate space should be uniform. The two-dimensional puckering coordinates were gridded into 5329 ( $73^2$ ) bins of area  $2.5^\circ \times 2.5^\circ$ . The three-dimensional puckering coordinates were gridded into 389 017 ( $73^3$ ) bins of volume  $2.5^\circ \times 2.5^\circ \times 2.5^\circ$ .

We included our FEARCF module into the macromolecular program CHARMM<sup>20</sup> to calculate the effect of the perturbing forces generated from  $U(\xi)$  for torsional and chemical reaction coordinates.<sup>21,22</sup> We have generalized the method to multiple dimensions<sup>17</sup> and shown its effectiveness for calculating pucker free energies.<sup>19</sup> At each step of the simulation the biasing force for  $\theta_i$  applied to the atoms involved in the rotatable plane is calculated from the gradient of the reaction coordinate potential for that puckering coordinate, which is

$$-\frac{\partial U(\xi)}{\partial \theta_i} = F(\theta_i) \quad (4)$$

where the force  $F(\theta_i)$  is calculated as the partial derivative of  $\theta_i$  with respect to the applied biasing reaction coordinate potential. The result is that the  $i$ th ring plane is biased away from the areas it has sampled with a force opposite to the accumulated sampling density as shown in eqs 2, 3, and 4. When implemented in a molecular dynamics (MD) routine, the biasing force for each puckering coordinate is converted to an atomic force in Cartesian coordinates and added to the forces from the equilibrium Boltzmann dynamic forces applied to each atom. The biasing forces on each ring atom can be recovered from the reaction coordinate forces by recasting them in terms of the PMF as shown in eq 5.

$$\frac{\partial W(\xi)}{\partial \theta_i} = F(\theta_i) \quad (5)$$

The force can be applied to the atoms that make up the puckering reaction coordinate by using the chain rule to get the component forces  $\partial W(\xi)/\partial x_i$  applied to the ring atoms ( $x_i$ ). The total biasing force is calculated by summing the contributions from each reaction coordinate that is then applied to the ring atoms in Cartesian coordinates. This approach negates the need for a Jacobian correction.

At the start of the FEARCF simulations the reaction coordinate potential is zero. The resulting probability distribution is used as a first guess for  $U(\xi)$ , and the biasing forces derived from this are applied to the next simulation. This process continues iteratively until the pucker conformational space is uniformly sampled (i.e., reaching convergence). Figure 3a shows how the biasing forces can be applied to atoms that describe the  $\theta_1$  flap, to convert from a  ${}^4\text{E}$  to a  ${}^4\text{C}_1$  conformer of glucose. In this example, the angle between the reference plane and the  $\theta_1$  plane is initially  $17.36^\circ$  but is forced down to  $-35.26^\circ$  by applying forces to the appropriate atoms of the reference and  $\theta_1$  planes.

The sampling rate of the reaction coordinate space was further improved by summing the histograms from several biased simulations after weighting them appropriately using the weighted histogram analysis method (WHAM).<sup>23–25</sup> The WHAM equations are applied iteratively until the maximum tolerance between the previous and current iteration weighting coefficients is less than 0.001.

**3.2. Finding Stationary Points and Transition Paths.** The global minimum is where the free energy is 0.0 kcal/mol. Other minimum energy stationary points are located near the expected canonical conformer positions. These minima are cells  $A, B, C, \dots$  in the gridded surface/volume that are lower in energy than all directly neighboring cells ( $N(A)_i, N(B)_j, N(C)_k, \dots$ ).

Paths between pairs of minima (e.g.,  $A$  and  $B$ ) follow the smallest change from  $A$  to  $B$ . This is not the shortest path between  $A$  and  $B$  since as any neighboring cell ( $P_i$ ) pointing in the direction of  $B$  can be traversed

$$\gamma_i = \cos^{-1} \left( \frac{\vec{\alpha} \cdot \vec{\beta}_i}{|\vec{\alpha} \vec{\beta}_i|} \right) < \pi; \quad \vec{\alpha} = B - A; \quad \vec{\beta}_i = P_i - A \quad (6)$$

Cells making up the minimum pathway are visited only once.

### 3.3. Reducing Dimensionality with Boltzmann-Averaging.

Multidimensional free energy hypersurfaces (or equivalent) can be reduced in dimensionality. For example, a free energy cubic volume could collapse into a free energy square surface by averaging over a chosen dimension. Simple averaging can be used, but this does not weight the chosen data appropriately along the coordinate. An alternative method is to use Boltzmann-averaging. To reduce from three spatial coordinates to one spatial coordinate, the following expression is applied

$$W(\theta_0)_{\theta_1, \theta_2} = \frac{\sum_{\theta_1, \theta_2} W(\theta_0, \theta_1, \theta_2) e^{-W(\theta_0, \theta_1, \theta_2)/k_B T}}{\sum_{\theta_1, \theta_2} e^{-W(\theta_0, \theta_1, \theta_2)/k_B T}} \quad (7)$$

where  $k_B$  is Boltzmann's constant,  $T$  is the temperature in kelvin, and  $W(\theta_0, \theta_1, \theta_2)$  is the multidimensional free energy calculated from simulations. An analogous expression applies for reduction of two spatial coordinates to one spatial coordinate.

#### 4. Simulation Details

For both the furanose and pyranose model sugars, a series of simulations were carried out with AM1,<sup>9</sup> PM3,<sup>10</sup> PM3CARB-1,<sup>11</sup> and SCC-DFTB<sup>12</sup> semiempirical potentials. Both the AM1 and PM3 potentials have been used for simulating carbohydrates.<sup>26–29</sup> The PM3CARB-1<sup>11</sup> parameters were developed to more accurately model carbohydrates and have been used to investigate the reasons for glucose's and galactose's primary alcohol rotamer populations in water.<sup>30</sup> The SCC-DFTB has recently become a popular method for QM/MM molecular simulations<sup>29,31,32</sup> including carbohydrates.

For both  $\beta$ -D-ribose and  $\beta$ -D-glucose, 20 iterations of QM/MM dynamics were carried out using CHARMM<sup>20</sup> v33b2. At each iteration eight PMF calculations of 0.8 ns in length were run using velocity-Verlet dynamics at 298.15 K with group-based cutoffs of 10, 12, and 14 Å. The electrostatics were treated with force switching, and the van der Waals potentials were shifted to account for long distance nonbonded interaction discontinuities. The nonbonded interactions were updated using CHARMM's built-in heuristic algorithm. The AM1 and PM3 modules (CHARMM version 33b2) were used while we implemented PM3CARB-1 based on the PM3 semiempirical routine and by adding the modified parameters with the EXTE function.<sup>30</sup> The REMO keyword was used to remove MM energies. SCC-DFTB calculations were run with the mro-0-1<sup>12</sup> parameters and an improvement to hydrogen-bonding interaction was included with the HBON keyword.

**4.1. DFT Energies of Selected Conformers.** Canonical conformers of ribose and glucose were extracted from FEARCF simulation trajectories. Bearing in mind that the primary alcohol hydrogen-bonding interaction can dramatically stabilize the energy of a conformer,<sup>30</sup> the “native” extracted coordinates were used in addition to coordinates where the primary alcohol ( $O_5-C_5-C_6-O_6$ ) was rotated into each of the three (trans-gauche, gauche-gauche, gauche-trans) staggered rotamers.

Each conformer was then optimized and the energy evaluated for AM1, PM3, PM3CARB-1, and SCC-DFTB. These energies were compared with the same conformations which were optimized with RB3LYP/6-311++G(d,p). We optimized the DFT structures using methods as prescribed by Momany et al.<sup>33,34</sup> based on the suggestion of Csonka.<sup>35</sup>

#### 5. Results

**5.1. Ribose.** For the furanose ring, the free energy is a function of  $(\theta_o, \theta_1)$ . The central and rotatable planes were chosen as described in section 2 and shown in Figure 3b. The pucker coordinates can be mapped to the ribose (10 envelope (E), 10 twist (T), and 1 planar) canonical conformers as illustrated in Scheme 1 and listed in Table 1. Scheme 1 shows a star-shaped line diagram indicating the directions along which furanose conformers exist in relation to the rotatable plane angles  $\theta_o$  and  $\theta_1$ . The nodes on the lines represent the  $\theta_o$  and  $\theta_1$  puckering coordinates that describe the ideal canonical envelope and twist conformers for cyclopentane (derived similarly to Hill et al.<sup>15</sup>). Each line represents varying degrees of pucker for that conformer starting from the planar conformer at the origin ( $0^\circ, 0^\circ$ ). For example, the E<sub>2</sub> conformer has the C2 atom below the plane of ring atoms (C3–C4–O4–C1). The characterization of this conformer as E<sub>2</sub> does not define the extent to which the C2 atom is beneath the ring plane. The conformers of the cyclopentane structures found, describe geometrically “ideal” canonical conformers where each ring atom can distort above or below the plane equally. In heteroatomic cyclic systems, such as carbohydrates, the canonical conformers may be described

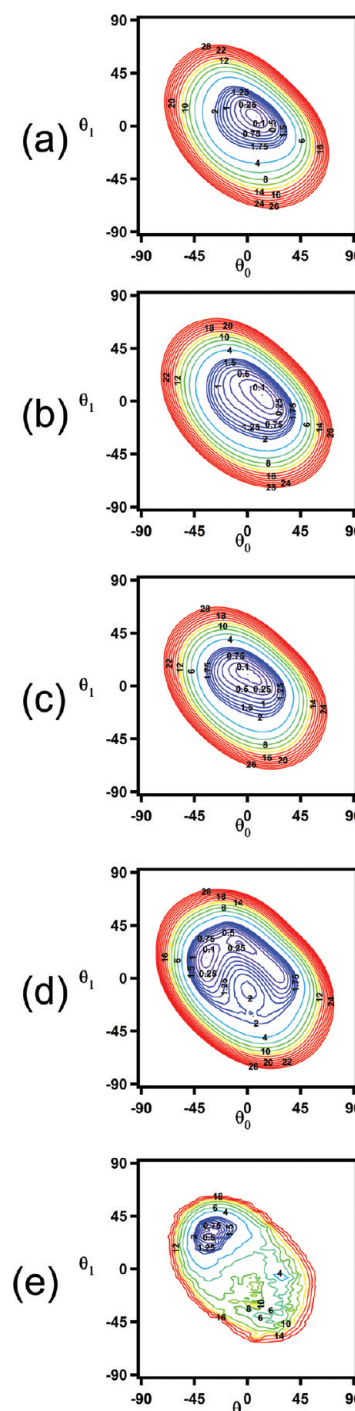


**Figure 4.** Furanose free energy of puckering shown as two-dimensional contour plots for (a) AM1, (b) PM3, (c) PM3CARB-1, (d) SCC-DFTB, and (e) HF 6-31G. The Hartree–Fock surface is not completely converged and has been smoothed twice. Energy has been mapped to color from 0 kcal/mol (blue) to 15 kcal/mol (red). Contours are shown at 0.1 kcal/mol; every 0.25 kcal/mol until 2 kcal/mol and every 2 kcal/mol thereafter.

in a series of possible  $\theta_o$  and  $\theta_1$  puckering coordinates represented by the labeled lines. In Figure 4, five contour plots of  $W(\theta_o, \theta_1)$  are shown for (a) AM1, (b) PM3, (c) PM3CARB-1, (d) SCC-DFTB, and (e) HF 6-31G with contours drawn at 0.1 kcal/mol, in increments of 0.25 kcal/mol until 2 kcal/mol, after which they are contoured every 2 kcal/mol. The energy is represented in color using a rainbow color scale where blue represents low energies (starting at 0 kcal/mol) and red high energies (up to 15 kcal/mol).

The AM1 free energy surface (Figure 4a) has a global minimum at ( $\theta_0 = 7.5^\circ$ ,  $\theta_1 = 7.5^\circ$ ) which is an  $E_o$  conformation. At 0.01 kcal/mol the  $^1T_o$  conformation, which borders the  $E_o$  conformation appears. These conformations and several others ( $^4T_o$ ,  $^1E$ ,  $^1T_2$ ,  $E_2$ ,  $^3T_2$ ,  $E_3$ ,  $^4T_3$ ,  $^4E$ , and planar) lie in a well 0.5 kcal/mol from the global minimum. There are no other stationary states on the free energy surface. Consequently, even though the deviations of the two planes C3–C4–O4 and O4–C1–C2 are greater for the  $^4T_3$  and  $^1T_2/E_2$  conformations compared with  $^oT_1$  and  $^oE$ , all conformers are readily accessible at room temperature at the AM1 level of theory. The planar conformer is located only 0.41 kcal/mol above the global minimum.

Conversely, the global minimum of the PM3 free energy landscape (Figure 4b) is a  $^4T_o$  conformation located at ( $12.5^\circ, 5.0^\circ$ ). There are no other stationary points in the close vicinity of  $^4T_o$ . There are, as in the AM1 case, several conformers accessible within 0.5 kcal/mol of the global minimum, with  $^3T_4$ ,  $E_4$ ,  $^oT_4$ ,  $^oE$ ,  $^oT_1$ ,  $E_1$ ,  $^2T_1$ , and  $^2E$  exhibiting the most distortion from the central planar structure. At 3 kcal/mol there is conformational interchangeability between all conformers. However, the energy required to pucker  $E_1$ ,  $^oT_1$ ,  $^oE$ ,  $E_o$ , and  $^1T_o$  away from the planar conformer is more than that for other conformers, which may imply that the ring oxygen prefers geometries that are more planar. In fact, the planar conformer is located at 0.3 kcal/mol above the global minimum compared with AM1 where it is found at 0.41 kcal/mol above that free energy global minimum.

The shape of the free energy surface for PM3CARB-1 (Figure 4c) is very similar to that of PM3 (Figure 4b). However, the lowest energy PM3CARB-1 conformer is not a  $^4T_o$  conformer as in PM3 but a  $^1E$  found at ( $0^\circ, 10^\circ$ ) with  $E_o$  at ( $5^\circ, 7.5^\circ$ ) within  $10^{-2}$  kcal/mol of it. Moreover, the transition separating these two conformations is less than 0.1 kcal/mol, making these structures energetically indistinguishable within the accuracy of these levels of theory. The planar conformer is found at 0.27 kcal/mol above the global minimum. Similar to the PM3 surface, all canonical conformers and the planar conformer can be accessed to some degree within an energy well of 0.5 kcal/mol. The conformers  $E_4$ ,  $^oT_4$ ,  $^oE$ ,  $^oT_1$ ,  $E_1$ ,  $^1T_o$ ,  $E_o$ , and  $^4T_o$  are not puckered close to the ideal cyclopentane topologies but instead are closer to the central planar geometry (see Scheme 1) relative to the rest of the conformers. The PM3 and PM3CARB-1 methods predict that the anomeric carbon may not easily tilt below the plane of the ring. While at 3 kcal/mol all conformers can be accessed, the shape of the minimum energy well dictates that the extent/magnitude of puckering of the structures in the  $E_3$  and  $^3T_2$  directions and adjacent to these is more than that of the  $^oT_1$ ,  $^1T_o$  conformers.

The furanose ring pucker free energy topologies calculated from AM1, PM3, and PM3CARB-1 (Figure 4a–c) are very similar to each other insofar that no significant distinction between the 21 different conformers exists. This is not the case for SCC-DFTB (Figure 4d). This semiempirical method reveals a difference in free energy between a number of ring pucker conformations. The surface shows several distinct conformational minima surrounding the global minimum at ( $-35^\circ, 17.5^\circ$ ). This global minimum is a  $^3E$  conformer with some  $^3T_4$  character. This conformer does facilitate hyperconjugation required to stabilize the TS oxocarbenium ion. These stationary points include a  $^1T_2$  minimum conformer at ( $-5^\circ, 30^\circ$ ) that is very similar in energy (0.08 kcal/mol) to  $^3E$  which can be accessed via an  $E_2/^3T_2$  transition point ( $-20^\circ, 27.5^\circ$ ) of 0.29 kcal/mol. There is a further minimum of 0.27 kcal/mol at ( $20^\circ, 10^\circ$ ) which is a  $^4T_o$  conformer. The  $^4T_o$  can be reached from  $^1T_2$  via an  $E_o$  transition of 0.31 kcal/mol at ( $15^\circ, 15^\circ$ ). Unlike the NDDO

**TABLE 3: A Comparison between AM1, PM3, PM3CARB-1, SCC-DFTB, and RB3LYP/6-311++G(d,p) Potential Energy Optimizations (Relative to Lowest Energy Conformer in kcal/mol) for  $\beta$ -D-Ribose**

	AM1	PM3	PM3CARB-1	SCC-DFTB	DFT optimized
from planar	0.52 <sup>c</sup>	2.14 <sup>c</sup>	0.00 <sup>c</sup>	optimizes out of planar conformer into $E_4$ , $^4E$ , $^4T_o$	optimizes out of planar conformer into $E$ , $^3T_2$ , $E_2$
$^oE$	<i>b</i>	<i>b</i>	1.41	<i>b</i>	<i>b</i>
$E_4$	4.11	<i>b</i>	<i>b</i>	0.00	<i>b</i>
$^3T_4$	<i>b</i>	<i>b</i>	<i>b</i>	0.00	<i>b</i>
$^3E$	<i>b</i>	<i>b</i>	1.99	0.29	2.38
$^3T_2$	<i>b</i>	<i>b</i>	<i>b</i>	<i>b</i>	0.00
$E_2$	<i>b</i>	<i>b</i>	<i>b</i>	<i>b</i>	1.10
$^1T_2$	5.52	<i>b</i>	2.33	0	0.68
$^1E$	5.47	0.31	2.49	0.28	<i>b</i>
$^1T_o$	0.00	0.28	0.82	0.29	<i>b</i>
$E_o$	0.42	0.28	0.29	0.38	<i>b</i>
$^4T_o$	2.44	0.00	0.00	0.46	0.57
$^4E$	1.88	1.16	2.73	0.27	0.44

<sup>a</sup> All conformers extracted from FEARCF dynamics simulations. The same canonical conformers used for optimizations at each level of theory. <sup>b</sup> Do not exist after optimization. <sup>c</sup> The lowest energy conformer that the planar conformer optimizes to and that is very close to planar. These are AM1 ( $9.7^\circ, 5.6^\circ$ ); PM3 ( $6.1^\circ, 3.9^\circ$ ); PM3CARB-1 ( $11.5^\circ, 3.1^\circ$ ).

semiempirical methods, which allow the furanose ring to pucker into the planar conformer requiring less than 0.5 kcal/mol, the SCC-DFTB method produces a planar conformer (1.91 kcal/mol) that is more than  $3kT$  above the global minimum. Therefore, while the planar conformer is accessible, it should be rarely observed at  $T = 298$  K.

AM1, PM3, and PM3CARB-1 all exhibit a large minimum energy well and no distinct global minimum. No significant energetic selectivity that discriminates between different pucker-conformers is evident, and all conformers are thermally accessible at  $6kT$ . Nonetheless, while all the conformers lie within the low free energy envelope, it is energetically more difficult to pucker  $^oT_1$ ,  $E_1$ ,  $^oE$ ,  $E_o$ , and  $^1T_o$  into their ideal conformer geometries than for other conformers shown in Scheme 1. The SCC-DFTB-produced furanose free energy pucker surface is strikingly different from that generated from the NDDO methods since an energetically variegated minimum well exists within the  $6kT$  free energy envelope. This implies that when treated with this level of theory the furanose ring can be puckered relatively easily at room temperature into discrete conformations.

Each of the IUPAC defined canonical conformers was extracted from the FEARCF AM1, PM3, PM3CARB-1, and SCC-DFTB free energy simulations and optimized at both that level of theory and separately using DFT RB3LYP/6-311++G(d,p). Table 3 lists conformers and energies obtained from these optimizations. The planar conformer was not stable for SCC-DFTB or DFT methods. While the DFT RB3LYP/6-311++G(d,p) treatment produces a  $^3T_2$  minimum (the pucker in between  $E_2$  and  $^3E$ ), none of the semiempirical free energy surfaces had this conformer as a global minimum. SCC-DFTB shows a  $^3T_4$  global minimum that occupies the same northwestern quadrant of Scheme 1 as does the  $^3T_2$  of DFT. The  $^1T_o$  of AM1,  $^4T_o$  of PM3, and  $^1E$  and  $E_o$  of PM3CARB-1 occupy the northeastern quadrant of Scheme 1 and are not similar to  $^3T_2$ . Here it is interesting to note that an analysis of crystallographically observed puckering for ribose sugars found stable  $^2E$ ,  $E_2$ ,  $^3E$ ,  $E_3$ , and  $E_4$  conformers. The minimum energy conformer of

**TABLE 4: Triangular Decomposition Pucker Coordinates (in deg) for Boltzmann-Averaged Minima vs the Actual 2D Minima for AM1, PM3, PM3CARB-1, and SCC-DFTB of Ribose<sup>a</sup>**

	AM1	PM3	PM3CARB-1	SCC-DFTB
min( $\theta_0$ )	10.0	15.0	0.0	-35
min( $\theta_1$ )	5.0	5.0	10.0	25
min( $\theta_0, \theta_1$ )	(7.5, 7.5)	(12.5, 5.0)	(0.0, 10)	(-35, 17.5)
max( $\theta_0$ )	-57.5; 60	-62.5; 62.5	-60; -60	-70; -67.5
max( $\theta_1$ )	-60; 60	-62.5; 60	57.5; 57.5	65; 67.5

<sup>a</sup> The coordinate values at an energy of 15 kcal/mol (so called “maxima”) are listed along with the minima.

ribose found by Jalbout<sup>36</sup> using CCSD(T)/6-31G\*\*//MP2/6-31G\*\* is an E<sub>2</sub> with an E<sub>3</sub> conformer located within 1 kcal/mol from it.

A partially converged free energy surface using Hartree–Fock (HF) theory (Figure 4e) has been used to calculate the free energy of ring pucker. Even though the HF surface is not as well sampled as the semiempirical surfaces, it reveals distinct minima for canonical pucker conformer states. This is in agreement with the SCC-DFTB surface and contradicts the pucker free energy surfaces that were produced using AM1, PM3, and PM3CARB-1. The HF surface shows <sup>3</sup>E (-35°, 30°) as the global minimum with a second minimum <sup>4</sup>T<sub>3</sub> at (27.5°, -7.5°) that is 1.02 kcal/mol higher on the FE surface. Other stationary points that feature on the HF FE surface are an 8.09 kcal/mol high-energy <sup>9</sup>T<sub>1</sub> conformer at (-7.5°, 17.9°) and a low-energy <sup>9</sup>T<sub>1</sub> conformer at (-12.5°, -32.5°). The overall shape of the FE surface bears some resemblance to SCC-DFTB, particularly the global minimum conformer <sup>3</sup>E that is similar to that observed in the solid state for the substituted ribose ring in phenylalanine tRNA.<sup>37</sup> Despite the lack of electron correlation in the HF calculation, this remains a promising result implying that for furanose systems SCC-DFTB bears a closer resemblance to *ab initio* methods than do AM1, PM3, and PM3CARB-1.

Pucker free energies and potential energies are often studied in a single dimension to, for example, arrive at a “minimum transition pathway” connecting two equilibrium wells. To illustrate the effect that a reduction in dimensionality has on the conformational analysis of carbohydrate rings, we use Boltzmann-averaging to contract the two-dimensional ( $\theta_0, \theta_1$ ) furanose surfaces to one dimension. Boltzmann-averaging over  $\theta_1$  yields a free energy coordinate as a function of  $\theta_0$ . As an example of the effect of a reduction in dimension, we analyze AM1 more closely and observe that the  $W(\theta_0)_{\theta_1}$  minimum occurs at 10° and rises to 10 kcal/mol at  $\theta_0 = \pm 50^\circ$ . On the other hand, averaging over  $\theta_0$  gives  $W(\theta_1)_{\theta_0}$  where the minimum occurs at 5° and the free energy rises to 10 kcal/mol at about  $\theta_1 = \pm 52.5^\circ$ . Comparing both 1D curves to the 2D free energy surface, it is clear that the position of the global minimum shifts to either side of the 2D global minimum position observed at (7.5°, 7.5°). The more serious problem of dimension reduction is the collation of nondegenerate conformers into single averaged points in conformational space. This is apparent as shown here for the AM1 furanose surface, which by all accounts is relatively simple, displaying very little character. The topologies of the 1D curves and 2D surfaces are listed in Table 4 to further illustrate the information penalty due to dimension reduction of complex pucker conformational space. This difference between 1D and 2D topologies is most severe for SCC-DFTB, which is the surface with the most character.

A check for free energy surface convergence is usually done by evaluating a simulation that has biasing forces applied to it

that are derived from the free energy surface. If the system has converged to the true free energy, then it will be driven away from parts of the reaction coordinates that are local minima on the equilibrium surface. The result is equal sampling across reaction coordinate space if the space is closed (e.g., angles, distances, etc.). Ring puckering has a closed canonical conformational space<sup>19</sup> with respect to the Hill–Reilly coordinates that is bounded by unphysical geometries (e.g., rings are twisted or folded into shapes that resemble pretzels) that are not easily sampled as they are very high in energy. In this case, the extent of convergence can be gauged by comparing the sampling of high energy conformers with that of the global minimum pucker sampling. A ratio of less than 50:1 is considered good,<sup>38,39</sup> and the surface is determined to be converged when this criterion is met. In the case of ribose the ratio of most to least sampled conformer for AM1 is 4:1, PM3 is 6:1, PM3CARB-1 is 7:1, and SCC-DFTB is 8:1.

**5.2. Glucose.** The free energy landscape of glucose puckering is necessarily more complex than that of ribose. Its free energy is a function of at least three degrees of freedom; the three puckering angles make up the reaction coordinate  $\xi_{\text{glucose}}$ . The choice to monitor the motion of the planes C4–C5–O5 ( $\theta_0$ ), O5–C1–C2 ( $\theta_1$ ), and C2–C3–C4 ( $\theta_2$ ) differs from those chosen by Hill and Reilly but allow observation of the contribution of the primary alcohol and anomeric carbon to the overall pyranose pucker free energy.

The more complex four-dimensional free energy landscape for hexoses can be visualized in three dimensions by representing the free energy as a color variable. Here the color scale represents low energies (0 kcal/mol) as blue and very high energies as red (15 kcal/mol). Although all simulations sampled regions up to and beyond ~30 kcal/mol, the structures in these regions are distorted high-energy conformers that are not chemically interesting (e.g., tightly bent, twisted, and scrunched up rings) and therefore not part of IUPAC canonical space definitions. The 38 canonical conformers categorizing six-membered rings are shown in a Hill–Reilly coordinate frame with respect to a chosen reference plane (Scheme 2) with the values for  $\theta_0$ ,  $\theta_1$ , and  $\theta_2$  listed in Table 2. While the complete volume is cubic in shape, i.e.,  $\theta_0, \theta_1, \theta_2 \in [-90^\circ, 90^\circ]$  the canonical conformers lie within a spherically shaped region. This spherical region is similar in appearance to the one used by Cremer and Pople (who mapped  $q_2$ ,  $q_3$ ,  $\phi$  to spherical coordinate space). The chairs (C) are the “poles” (<sup>1</sup>C<sub>4</sub> north and <sup>4</sup>C<sub>1</sub> south) while the equator contains all possible boat (B) and twist/skew (S) canonical conformers. The northern or axial tropic contains half-chair (H) and envelope (E) conformations that are accessible from the <sup>1</sup>C<sub>4</sub> chair, while the southern or equatorial tropic contains H and E conformations that neighbor the <sup>4</sup>C<sub>1</sub> chair.

In each of the  $W(\theta_0, \theta_1, \theta_2)$  landscapes (AM1 through SCC-DFTB), an inner isovolume (deep blue) at 3 kcal/mol represents the pucker conformers which can be accessed at  $\sim 6kT$ . The lowest energy conformer is <sup>4</sup>C<sub>1</sub> in all cases (Figure 5). The free energy volumes calculated using the original NDDO methods (AM1 and PM3) imply that the pyranose ring is easily deformed (Figure 5, a and b). An exchange between <sup>4</sup>C<sub>1</sub> and <sup>1</sup>C<sub>4</sub> requires only about 4 kcal/mol for both levels of theory. The 3 kcal/mol energy isosurface for AM1 shows all twist and boat conformers (i.e., <sup>0,3</sup>B, <sup>0</sup>S<sub>2</sub>, B<sub>2,5</sub>, <sup>1</sup>S<sub>5</sub>, <sup>1,4</sup>B, <sup>1</sup>S<sub>3</sub>, B<sub>0,3</sub>, <sup>2</sup>S<sub>0</sub>, <sup>2,5</sup>B, <sup>5</sup>S<sub>1</sub>) at room temperature except <sup>3</sup>S<sub>1</sub> and B<sub>1,4</sub>. In the PM3 case a large number of boat and twist conformers (B<sub>0,3</sub>, <sup>2</sup>S<sub>0</sub>, <sup>2,5</sup>B, <sup>5</sup>S<sub>1</sub>, <sup>3</sup>S<sub>1</sub>, <sup>0,3</sup>B, <sup>0</sup>S<sub>2</sub>, B<sub>2,5</sub>, <sup>1</sup>S<sub>5</sub>, and a very restricted B<sub>1,4</sub>) are seen within the 3 kcal/mol free energy volume well. There appears to be an easy

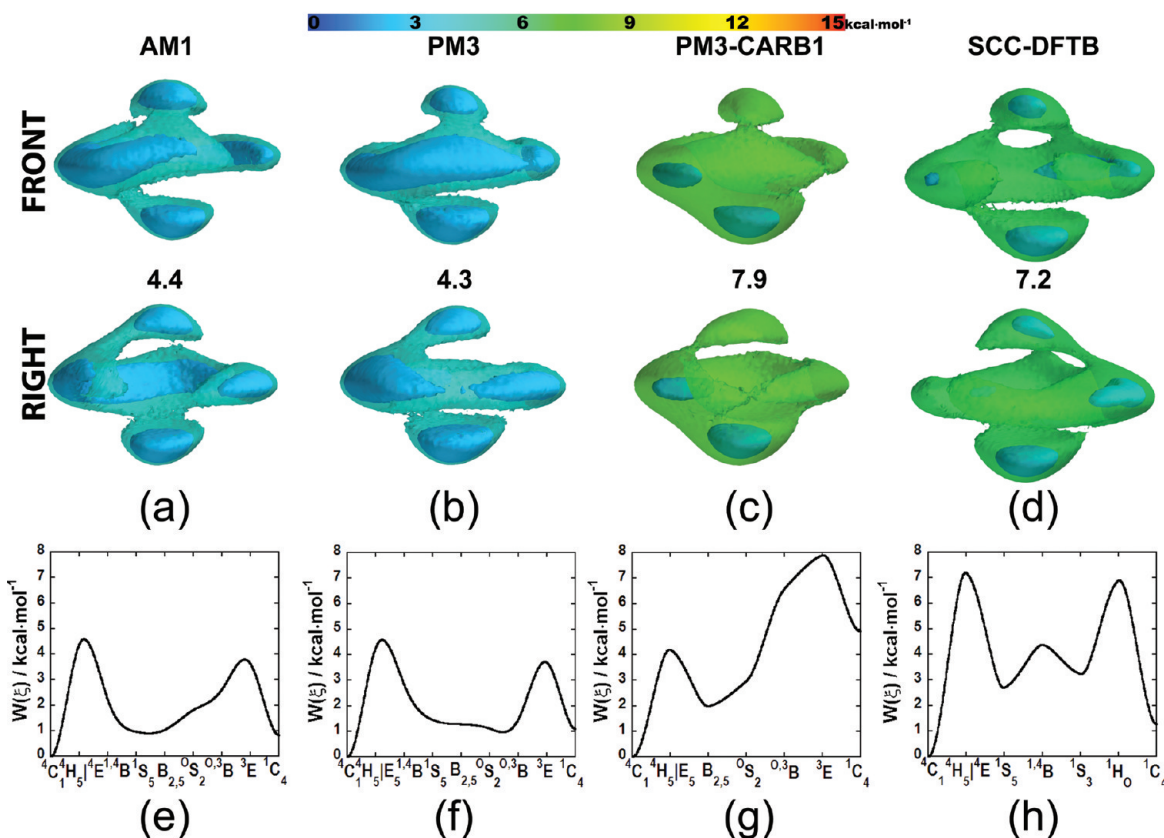


**Figure 5.** Free energy of puckering color mapped to three-dimensional volumes for (a) AM1 (mapped to color from 0 kcal/mol (blue) to 15 kcal/mol (red)). The inner isosurface is at 3 kcal/mol and the outer isosurface indicating the minimum free energy to connect the “poles” ( $^1\text{C}_1$ ,  $^4\text{C}_1$ ) occurs at (a) 4.4, (b) 4.3, (c) 7.9, (d) 7.2 kcal/mol, respectively. The minimum free energy paths between the equatorial chair ( $^4\text{C}_1$ ) and axial chair ( $^1\text{C}_4$ ) have been extracted from the free energy volumes (a–d) and represented for (e) AM1, (f) PM3, (g) PM3CARB-1, and (h) SCC-DFTB.

exchange between  $\text{B}_{0,3}$ ,  $^2\text{S}_0$ ,  $^{2,5}\text{B}$ , and  $^5\text{S}_1$ . Similarly, transitions between  $^1\text{S}_5$ ,  $\text{B}_{2,5}$ ,  $^0\text{S}_2$ ,  $^{0,3}\text{B}$ , and  $^3\text{S}_1$  are feasible.

Using PM3CARB-1, the parameter set that was especially modified to model carbohydrates, we observe a greater restriction of pyranose pucker (Figure 5c) compared with AM1 and PM3. While  $^4\text{C}_1$  is the global minimum, contouring at 3 kcal/mol shows only this conformer and a pathway between two other conformers ( $^1\text{S}_5$  and  $\text{B}_{2,5}$ ) at the equator to be possible. There is no path to the other chair ( $^1\text{C}_4$ ) observable at room temperature since more than  $6kT$  separate them.

While SCC-DFTB does not display the almost floppy pyranose ring seen in AM1 and PM3 treatments, it is not nearly as conformationally restricted as the PM3CARB-1 model at 3 kcal/mol. At this contour, both chair conformers are accessible but not equally so, as the volume about  $^1\text{C}_4$  is marginally smaller than that about  $^4\text{C}_1$ . Five canonical conformers at the equator are observed with  $^1\text{S}_5$  showing up as being isolated at this contour where easy interchange between  $\text{B}_{0,3}$ ,  $^2\text{S}_0$ ,  $^{2,5}\text{B}$ , and  $^5\text{S}_1$  appears to be possible.

The conformational path from the  $^4\text{C}_1$  conformer, where all the glucose hydroxyls are equatorial, to the  $^1\text{C}_4$ , where all the hydroxyls are axial, goes via strained conformers that differ in energy from one semiempirical method to another. The barrier heights separating  $^4\text{C}_1$  from  $^1\text{C}_4$  for AM1 and PM3 are quite similar (i.e., 4.4 and 4.3 kcal/mol, respectively) while the PM3CARB-1 and SCC-DFTB methods have barrier heights that are nearly twice as high with values of 7.9 and 7.2 kcal/mol, respectively. The isosurfaces corresponding to this energy are

shown as free energy volume plots that can be projected onto the schematic diagram for pyranose rings (Scheme 2) and are shown in Figure 5a–d.

Minimum free energy paths have been extracted and plotted as line diagrams (Figure 5e–h). In the line diagrams the minimum energy paths are shown while the isosurfaces detail all conformers available for free energies at and below the contour level shown. Starting from  $^4\text{C}_1$  using the AM1 level of theory and driving northward, the chair distorts into  $^4\text{H}_3$ ,  $^4\text{E}$ , and  $^4\text{H}_5$  after which these ring conformers can easily alter into the  $^1\text{S}_3$ ,  $^{1,4}\text{B}$ , and  $^1\text{S}_5$  conformations (although  $^4\text{H}_3$  and  $^1\text{S}_3$ , are not on the minimum free energy path). At the equator,  $^1\text{S}_5$  is lowest in energy and all conformers but  $\text{B}_{1,4}$  are accessible. The connection to the  $^1\text{C}_4$  conformer can be made from the  $^0\text{S}_2$ ,  $^{0,3}\text{B}$ , or  $^3\text{S}_1$  structure via the  $^3\text{H}_2/{}^3\text{E}$  bridge where  $^0\text{S}_2$  is lowest in energy ( $^3\text{S}_1$  is not on the minimum free energy path). The minimum energy path is shown in Figure 5e.

In the PM3 case, the route from  $^4\text{C}_1$  to  $^1\text{C}_4$  occurs via the  $\text{E}_5/{}^4\text{H}_5$  conformers through the  $\text{B}_{2,5}$  or  $^1\text{S}_5$  conformers with  $\text{B}_{2,5}$  being slightly lower in energy than  $^1\text{S}_5$  (a difference of less than 1 kcal/mol). The  $^1\text{C}_4$  conformer is reached via  $^3\text{E}$  or  $^3\text{H}_4$  from the  $^{0,3}\text{B}$  conformer. Here, all conformers located on the equator (Scheme 2) can be reached from the chair conformations requiring no more than 3 kcal/mol.

PM3CARB-1 shows a distinctly different minimum path between the  $^4\text{C}_1$  and  $^1\text{C}_4$  conformers. The lowest energy conformer that can be used to access the equator from  $^4\text{C}_1$  is  $^4\text{H}_5$  with some  $\text{E}_5$  character. Following this, the  $^1\text{S}_5$ ,  $\text{B}_{2,5}$ , and

$^0S_2$  can be accessed with the lowest energy conformer being  $^1S_5$  (although it is not on the shortest minimum energy path). The route to  $^1C_4$  is through the  $^3E/{}^3H_2$  conformers via  ${}^0{}^3B$ . This free energy volume is very different from the AM1 and PM3 volumes as all envelopes and half-chairs near  $^4C_1$  are energetically accessible when using original NDDO parameter sets as implemented in CHARMM. Furthermore, all but the  $E_1$ ,  ${}^2H_1$ , and  ${}^2E$  envelopes and half-chairs provide a direct path to the skew boats and boat conformers. For PM3CARB-1 it is easier to transform  $^4C_1$  to conformations found at the equator of the pyranose spherical pucker volume than it is for  $^1C_4$ . There are sometimes multiple paths of similar energy connecting the poles to the equator. For example in SCC-DFTB, the  $^1C_4$  to equator transition can occur via  ${}^1H_0$  or  ${}^5H_0$  which are similar in energy at  $\sim 7$  kcal/mol.

By use of the SCC-DFTB level of theory, the  $^4C_1$  conformer can be transformed into  $^1S_5$  and  ${}^1{}^4B$  conformers via a  ${}^4E$  state. Once in the S/B conformations, the  $^1C_4$  conformer can be reached via a  ${}^5H_0$  or  ${}^1H_0$  conformation. While the  ${}^1H_0$  conformer presents the shorter conformational route, a transformation via  ${}^5H_0$  is slightly lower in energy. Most boats and twist boats are energetically accessible within the 7.2 kcal/mol energy volume. It is not possible to reach the canonical  ${}^0{}^5B$  located at the equator of the pucker sphere at this energy, nor the  ${}^4E$ ,  ${}^0H_5$ , and  ${}^0H_1$  that are positioned at the “tropics” of the sphere shown in Scheme 2. There is only one possible transition at this contour from  $^4C_1$  to the boat and twist boat conformers while two such paths exist when starting at the  $^1C_4$  chair.

There have been several theoretical studies investigating the energetic differences of ring puckers for glucose and selected derivatives.<sup>1,40</sup> While it would be ideal to employ *ab initio* methods to construct the free energy volumes, this is not within reach of current computational methods and hardware. We are, however, able to evaluate the semiempirical methods used here against calculations done for selected conformers. An example of such a case is the work of Ionescu et al.<sup>40</sup> who carried out dynamical density functional theory (DFT) calculations with the projector augmented-wave (PAW) method and found that the transition state for permethylated glucose from the  $^1C_4$  chair to  ${}^1{}^4B$  was an  ${}^1E$  envelope conformation. Consequently, from the envelope-like transition state, the system evolved into the  ${}^1{}^4B$  minimum (this is a TS for the SCC-DFTB and other semiempirical methods investigated here). They found a  ${}^1S_5$  skew-boat minimum and discovered that pucker pseudorotation stopped before the  ${}^0S_2$  skew-boat was reached. The transition state to the inverted  $^4C_1$  chair was a mix of envelope and half-chair conformations. The energy barrier to leave the  $^4C_1$  chair minimum was 1.488 kcal/mol (7.2 kJ/mol), nearly twice the free-energy barrier required to make a transition from the  $^1C_4$  chair minimum.

The lowest optimized potential energy conformer for the AM1 and PM3 parameter set is the  $^1C_4$  conformer where secondary and primary hydroxyls are axial. This result does not correspond to RB3LYP/6-311++G(d,p) optimizations that show the lowest potential energy is due to the  $^4C_1$  conformer (Table 5). However, optimizations on the SCC-DFTB and PM3CARB-1 potential energy surface do correspond to this result. These two methods match the DFT potential energy surface more closely, although there are certain discrepancies. While, as with DFT, the PM3CARB-1 parameter set shows the  $^1C_4$  chair to be much higher in energy compared with the most favored  $^4C_1$  conformer, SCC-DFTB presents a small energy difference (1.24 kcal/mol) between the two chairs. Optimizations with DFT do not generate half-chair, envelope,  ${}^2{}^5B$ ,  $B_{2,5}$ , or  $B_{1,4}$  conformers, suggesting

TABLE 5: Comparison between AM1, PM3, PM3CARB-1, SCC-DFTB, and RB3LYP/6-311++G(d,p) Potential Energy Optimizations (Relative to Lowest Energy Conformer (in kcal/mol)) for  $\beta$ -D-Glucose

conformer	AM1	PM3	PM3CARB-1	SCC-DFTB	DFT optimized
${}^4C_1$	0.14	1.12	0.00	0.00	0.00
${}^1C_4$	0.00	0.00	4.68	1.24	7.14
${}^1S_5$	1.31 <sup>a</sup>	3.61 <sup>a</sup>	5.46 <sup>a</sup>	4.08 <sup>a</sup>	8.16 <sup>a</sup>
${}^5S_1$	5.36	3.99	7.90	5.14	9.96
${}^1S_3$	1.92	3.93	1.88	2.98	6.67
${}^3S_1$	3.70	3.05	6.62	3.24	7.20
$B_{0,3}$	1.11	2.63	1.59	3.48	5.46
${}^0{}^3B$	1.54	2.82	8.30	3.47	7.95
${}^0S_2$	1.79	3.40	5.59	1.29	9.73
${}^2S_o$	0.59 <sup>b</sup>	1.46	1.94	3.90	3.87

<sup>a</sup> Optimized from  ${}^1{}^4B$  indicating it is not a minimum on the potential energy surface. <sup>b</sup> Optimized from  ${}^1S_5$ .

these are not minimum energy stationary points. However, AM1 yields  $B_{2,5}$ ,  ${}^1H_2$ ,  ${}^5E$ , and  ${}^2{}^5B$ ; PM3 yields  $B_{2,5}$ ,  ${}^2{}^5B$ ,  $B_{1,4}$ ,  ${}^1H_2$ , and  ${}^3H_2$ ; PM3CARB-1 yields  ${}^3H_2$ ,  $E_2$ ,  ${}^5H_4$ , and  $B_{2,5}$ ; and SCC-DFTB yields  $B_{1,4}$  in addition to the conformers shown in Table 5. When comparing the stable conformers that SCC-DFTB optimizes to, the performance is closer to that of the DFT treatment, while NDDO methods optimize to minima further from the DFT potential surface.

Static conformational optimizations have severe limitations since they do not include the contributions of the many degrees of freedom (e.g., primary and secondary alcohol rotations, hydrogen bonding, etc.) to the pucker conformational space. The free energy volume is a useful measure of the relative stability of various ring puckers. To evaluate our results, we have to rely on the few reports<sup>19,41,42</sup> of complete free energy of the pucker volumes for pyranose rings that exist. Biarnés et al.<sup>41</sup> were able to sample only the southern hemisphere of the Cremer–Pople pucker volume using a metadynamics procedure. Sega et al. analyzed the metadynamics method used to calculate the Cremer–Pople pucker volume and concluded that, when Biarnés et al. attempted to traverse free energies using the Cremer–Pople Cartesian coordinates, they were limited to free energy barriers that were lower than the thermal energy at the equatorial (boat and skew conformers) region.<sup>42</sup> When analyzing the sampled hemisphere produced by the metadynamics simulation, it becomes apparent that the transition  ${}^4C_1 \rightarrow {}^1S_5/B_{0,3}$  goes via a  ${}^4H_3/E_3$ . This result is similar to that seen in all the semiempirical free energy volumes. However, when using static B3LYP/6-311++G\*\* calculations, Kurihara et al.<sup>43</sup> proposed the transition to be via  $E_3/{}^2H_3$  conformations. Davies et al. suggest that there is good evidence for the existence of  ${}^4H_3$ ,  ${}^3H_4$ ,  ${}^2{}^5B$ , and  $B_{2,5}$  TS pucks of the pyranose ring in glycosides.<sup>44</sup>

It was argued above that a reduction in the dimension of the free energy results in a significant loss of information. For a pyranose ring, a Boltzmann average over the motion of a single rotatable plane results in a two-dimensional free energy surface. Such surfaces are plotted as contour maps  $W(\theta_o, \theta_1)_{\theta_2}$ ,  $W(\theta_o, \theta_2)_{\theta_1}$ , and  $W(\theta_1, \theta_2)_{\theta_o}$  for AM1, PM3, PM3CARB-1, and SCC-DFTB in Figure 6. Both  ${}^4C_1$  chair and  ${}^1C_4$  chair structures can be distinctly seen for  $W(\theta_o, \theta_1)$  and  $W(\theta_o, \theta_2)$  and  $W(\theta_1, \theta_2)$  at  $\sim(-35^\circ, -35^\circ)$  and  $\sim(35^\circ, 35^\circ)$  for all methods, although the boat structures are included in the averaging. A cursory inspection of the 2D surfaces leaves one with the *incorrect* impression that all semiempirical levels of theory model the pyranose ring in the same way, with the only differences being some changes in barrier heights and minima of a couple of kcal/mol.

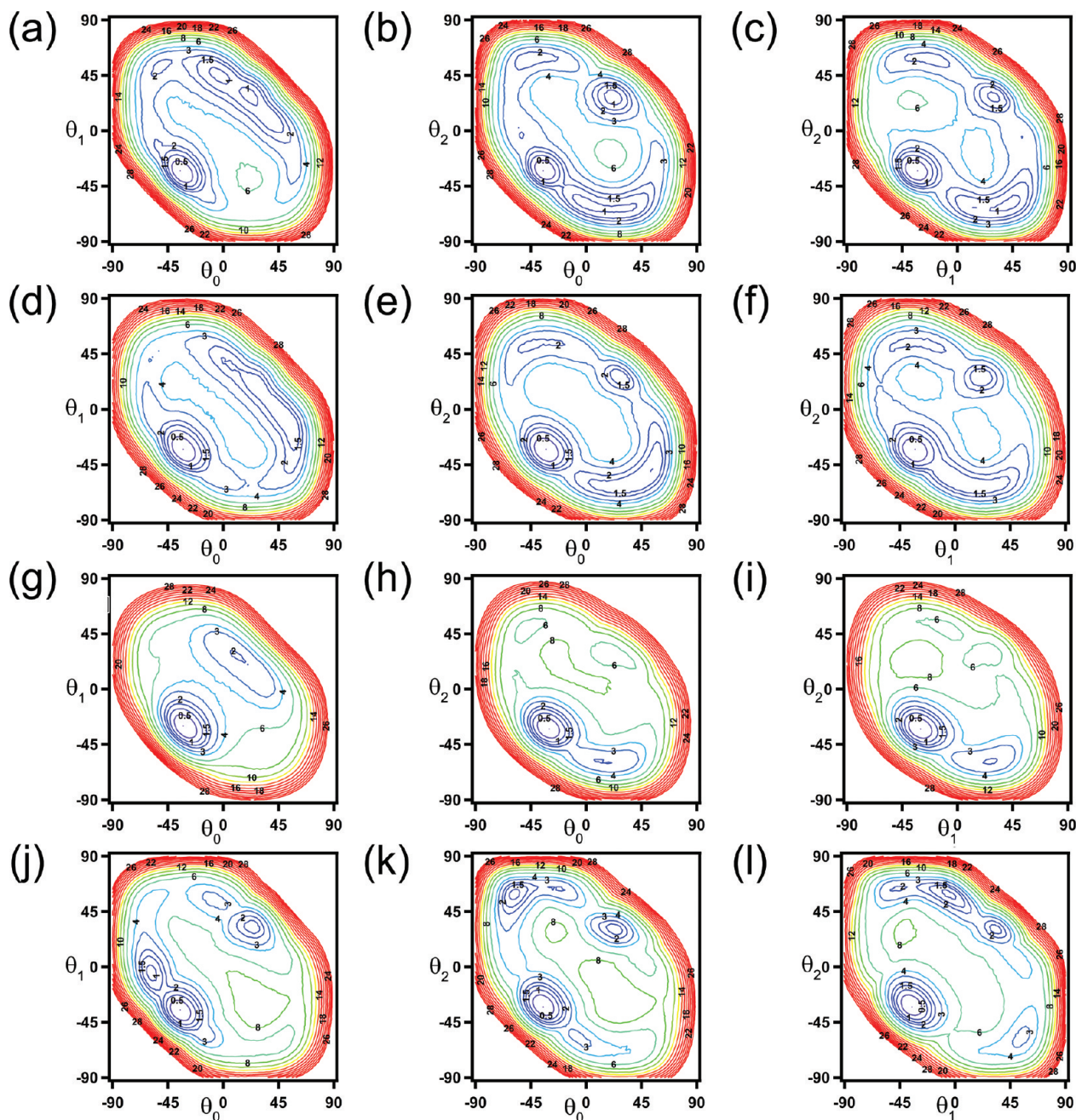


**Figure 6.** 2D free energy contour plots that are Boltzmann-averaged over a single dimension for  $\beta$ -D-glucose. For AM1 averaging the free energy  $W(\theta_0, \theta_1, \theta_2)$  yields (a)  $W(\theta_0, \theta_1)_{\theta_2}$ , (b)  $W(\theta_0, \theta_2)_{\theta_1}$ , and (c)  $W(\theta_1, \theta_2)_{\theta_0}$ . The same plots are shown for PM3 (d,e,f), PM3CARB-1 (g,h,i), and SCC-DFTB (j,k,l).

mol. Furthermore, in all of these plots the planar structure appears unresolved because it is averaged to a lower energy along with boat, envelope, twist boat, and half-chair structures. This is contrary to observations made in the 3D free energy volumes.

As in the complete free energy volumes for AM1 and PM3 (Figure 5, a and b), there are strong similarities in the surfaces (Figure 6a–f). The sugar specific parameter set, PM3CARB-1 (Figure 6g–i), produces surfaces that resemble AM1 (Figure 6a–c) and PM3 (Figure 6d–f) surfaces but with much higher energy barriers separating the minima. The ring pucker for the  $W(\theta_0, \theta_2)$  and  $W(\theta_1, \theta_2)$  cases appears more limited to the  $^4C_1$  chair. This minimum well is smaller than AM1, PM3, SCC-DFTB, indicating that the PM3CARB-1 potential allows pyranose rings far less conformational freedom compared with the other methods. However, the 2D surfaces do preserve the

underlying differences in topologies for SCC-DFTB compared with the other methods. The typical minimum ( $\sim -35^\circ, \sim -35^\circ$ ) that includes the  $^4C_1$  chair for all methods (Figures 6j–l) is observed but an additional minimum at ( $\theta_0 = -57.5^\circ, \theta_1 = -5^\circ$ ) showing possible E<sub>5</sub> envelope character (Figure 6j) is present. Minima at ( $\theta_0 = -6^\circ, \theta_1 = 57.5^\circ$ ), ( $\theta_0 = 25^\circ, \theta_1 = 32.5^\circ$ ) suggest  $^3H_2$  and a mixture of  $^1C_4$ , B<sub>1,4</sub>, and E<sub>4</sub>, respectively. Similar minima are seen in Figure 6k ( $\theta_0 = -58.5^\circ, \theta_2 = 57.5^\circ$ ); ( $\theta_0 = -20^\circ, \theta_2 = 65^\circ$ ); ( $\theta_0 = 20^\circ, \theta_2 = 32.5^\circ$ ), Figure 6l ( $\theta_1 = -40^\circ, \theta_2 = 65^\circ$ ); ( $\theta_1 = 0^\circ, \theta_2 = 57.5^\circ$ ); ( $\theta_1 = 35^\circ, \theta_2 = 32.5^\circ$ ); ( $\theta_1 = 52.5^\circ, \theta_2 = -60^\circ$ ), which are suggestive of the more intricate volume enjoyed by SCC-DFTB (Figure 5d).

A Boltzmann average over the motion of two rotatable plane results in one-dimensional plots  $W(\theta_0)_{\theta_1, \theta_2}$ ,  $W(\theta_1)_{\theta_0, \theta_2}$ , and  $W(\theta_2)_{\theta_0, \theta_1}$ . These plots provide very little information on the conformational preferences for pyranose rings (Figure 7) as there

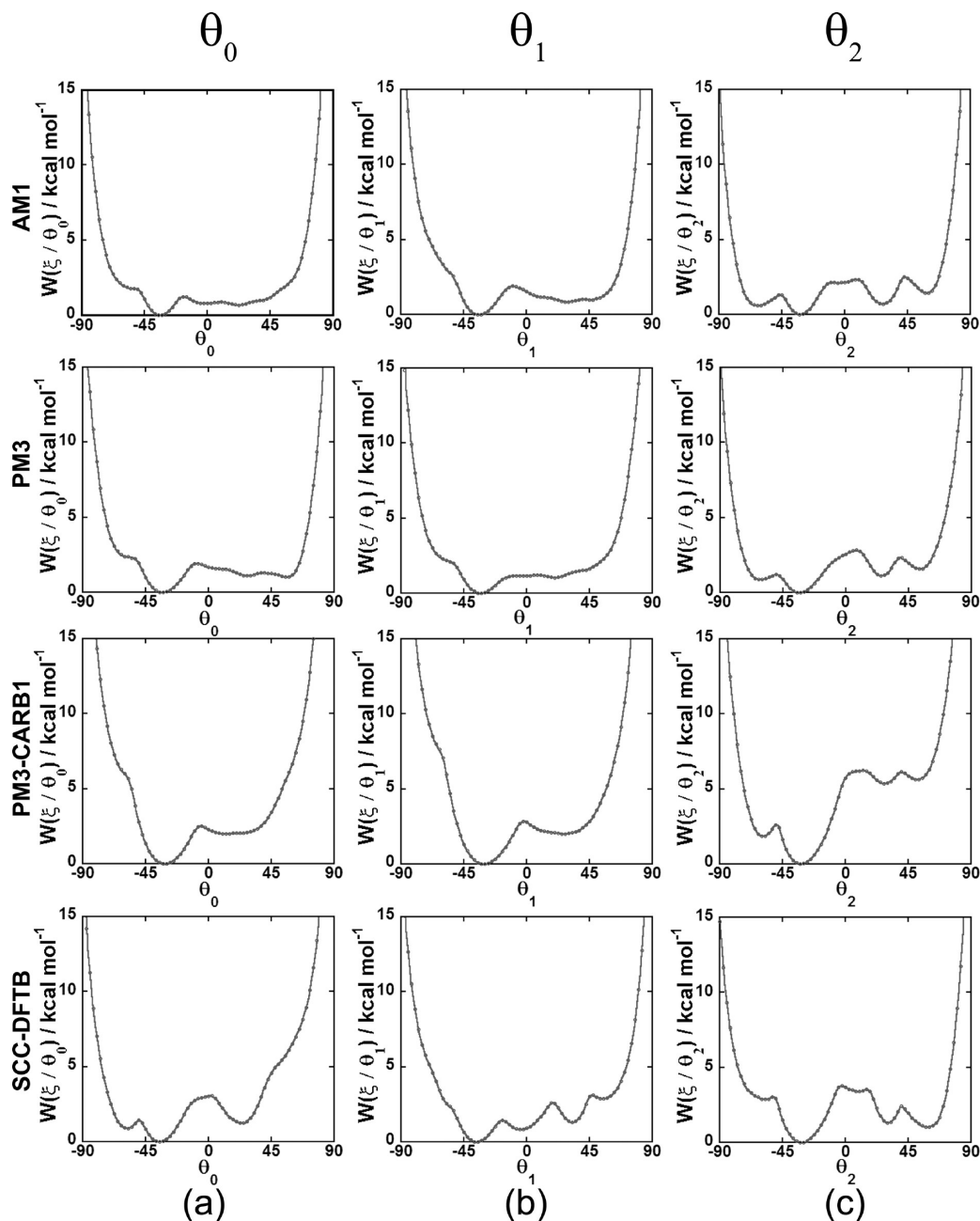


**Figure 7.** 1D free energy contour plots that are Boltzmann-averaged over two rotatable planes for  $\beta$ -D-glucose. The free energy  $W(\theta_o, \theta_1, \theta_2)$  averaged over  $\theta_1, \theta_2$  yields (a)  $W(\theta_o)_{\theta_1, \theta_2}$ , over  $\theta_o, \theta_2$  yields (b)  $W(\theta_1)_{\theta_o, \theta_2}$ , and over  $\theta_o, \theta_1$  yields (c)  $W(\theta_2)_{\theta_o, \theta_1}$ .

is not a 1:1 mapping between the energy and the conformer. These line drawings give the false impression of a one-dimensional free energy “path”. However, on comparison with the extracted lowest free energy paths, as shown in Figure 5e–h, it is clear that they bear no resemblance to a minimum free energy path. This illustration should serve as cautionary evidence when attempting to reduce complex ring puckering to lower dimensions. The reason as previously stated is that in particular the line graphs conflate pockers sharing coordinates in a reduced dimension even though they are energetically very different from each other. Once reduced, the contributing conformers and their associated free energies cannot be recovered from the average energy and averaged conformers making up the line graphs of Figure 7.

Despite the fact that they add little value to any investigation of puckering pathways and preferences, the  $W(\theta_o)_{\theta_1, \theta_2}$ ,  $W(\theta_1)_{\theta_o, \theta_2}$ , and  $W(\theta_2)_{\theta_o, \theta_1}$  line graphs do maintain some character observed

in the complete  $W(\theta_o, \theta_1, \theta_2)$  free energy volume. The graphs for AM1 (Figure 7a) and PM3 (Figure 7b) are very similar. AM1 shows a preference for  $\theta_o$  to be at  $-35^\circ$  and PM3 for  $\theta_o$  at  $-32.5^\circ$ . This is indicative of boat or chair structures. The energy increases rapidly to left of this region with a slight plateau/inflection at  $\theta_o = -55^\circ$ . At  $0^\circ$  there is a slight barrier. This includes the average of planar, boat, envelope, and even half-chair structures. Between  $0^\circ$  and  $60^\circ$ , there is a broad, poorly resolved region. PM3 shows a slight minimum at  $\theta_o = 50^\circ$  due to twist boat conformers.

As with  $W(\theta_o)_{\theta_1, \theta_2}$  and  $W(\theta_1)_{\theta_o, \theta_2}$ , the  $W(\theta_2)_{\theta_o, \theta_1}$  line graphs for AM1 and PM3 are similar with a minima at  $\theta_2 = -32.5^\circ$ . However, the PM3CARB-1 line graph is more asymmetric as was seen in the full 3D  $W(\theta_o, \theta_1, \theta_2)$  volume. PM3CARB-1 is similar to AM1 and PM3, with the important difference that with this potential there is a sharper increase in energy deviating from the minimum conformer. This indicates that the ring is

less flexible with the PM3CARB-1 potential. The minima for the three NDDO methods all lie at  $\theta_0 = -30^\circ$ ,  $\theta_1 = -30^\circ$ ,  $\theta_2 = -32.5^\circ$ . SCC-DFTB shows similar minima at  $\theta_0 = -35^\circ$ ,  $\theta_1 = -35^\circ$ ,  $\theta_2 = -32.5^\circ$ .

Previously, we compared the sampling of high energy conformers, such as the planar conformer, to the lowest energy conformer as a measure of the convergence of the pyranose free energy volume calculation. A ratio of less than 50:1 has been proposed to declare convergence<sup>38,39</sup> and thus that the volume is resolved. The free energy volumes shown here are well resolved, since the sampling of the planar conformer to the canonical conformers in the final iteration of calculation of the PMF are AM1 11:1; PM3 8:1; PM3CARB-1 15:1; and SCC-DFTB 10:1.

## 6. Conclusions

Carbohydrate ring puckering plays a central role in several biochemical processes such as hydrolysis, phosphorylation, and glycosylation reactions. Here, we have shown that semiempirical methods commonly used to simulate these reactions are mostly unsuitable, when modeling the ribose or glucose derivative ring puckering. In the case of ribose the NDDO methods (AM1, PM3, and PM3CARB-1) make little distinction between canonical ring conformers, displaying no stationary points on the free energy surface for any one pucker simulated at room temperature. We believe that simulations employing these methods and that then consequently derive conformational minima and transition states from them, lead to incorrect structures. In addition, these structures cannot be corrected by adjusting the energy with a calculation at a higher level of theory. However, the second-order expansion of the density functional theory method, the so-called SCC-DFTB method, produces a free energy surface that is very different from the NDDO methods and similar to the surface obtained with *ab initio* methods.

The glucose free energy volume for the AM1 and PM3 NDDO parameter sets result in an unrealistically flexible pyranose ring. At room temperature the preferred  $^4C_1$  conformer is easily distorted into half-chairs and boats. By contrast, the recently introduced PM3CARB-1 parameter set presents a rigid pyranose ring that shows very high barriers between the  $^4C_1$  conformer and the half-chairs and boats located at the equator of the free energy volume. The SCC-DFTB method compromises between the two extremes. Nonetheless, the SCC-DFTB free energy volume results in a  $^4C_1 \rightarrow ^1C_4$  minimum path that has barrier heights of the same magnitude (7 kcal/mol) as the path extracted from the PM3CARB-1 free energy volume. Of note is the wide range of minimum free energy pathways seen for the semiempirical methods investigated here. The  $^4C_1$ ,  $^1C_4$ ,  $^1S_5$ ,  $^2S_0$ ,  $^{2,5}B$ ,  $B_{0,3}$ , and  $^5S_1$  conformers are likely to be observed at room temperature when described by the SCC-DFTB method.

The  $^4H_5$  (and nearby  $^4E$  and  $^4H_3$  conformers), postulated to be a possible oxocarbenium TS conformer in glycosidases,<sup>44</sup> are found along the SCC-DFTB minimum free energy path from the  $^4C_1$  conformer to the equator. Other pucker conformers observed in enzymes include the  $^4E$ ,  $^1S_3$ , and  $^{2,5}B$  conformers.<sup>45–47</sup> According to SCC-DFTB, the enzyme active site may provide stabilizing interactions that overcome as much as 7.2 kcal/mol to prefer certain ring puckering conformations.

We find that the FEARCF method in combination with the Hill–Reilly pucker coordinates allow for complete exploration of the ribose and glucose free energy space. Here we caution that analyses of reduced free energy space will lead to severely approximated puckles with free energies that bear no relation to the actual values calculated using a minimum of  $N - 3$  ( $N$

= number of ring atoms) pucker coordinates. Finally, although it may still be far from the final goal, the SCC-DFTB performs better for prototypical furanose and pyranose systems than the NDDO methods, when we compare the relative energy of the optimized canonical conformers found from each semiempirical method with the energies of the same conformers optimized using DFT methods.

**Acknowledgment.** This work is based upon research supported by the South African Research Chairs Initiative (SARChI) of the Department of Science and Technology and National Research Foundation to K.J.N. C.B. thanks SARChI for doctoral support.

**Supporting Information Available:** Primary alcohol torsional angle for glucose data, corresponding to the pucker energies in Table 5, is available (Table S1). Time series plots of selected FEARCF trajectories showing the interconversion between primary alcohol rotamers are included (Figures S1–S4). The 1D Boltzmann-averaged free energies for ribose are also included (Figure S5). This material is available free of charge via the Internet at <http://pubs.acs.org>.

## References and Notes

- Fushinobu, S.; Mertz, B.; Hill, A. D.; Hidaka, M.; Kitaoka, M.; Reilly, P. J. *Carbohydr. Res.* **2008**, *343*, 1023.
- Johnson, G. P.; Petersen, L.; French, A. D.; Reilly, P. J. *Carbohydr. Res.* **2009**, *344*, 2157.
- Devi-Kesavan, L. S.; Gao, J. *J. Am. Chem. Soc.* **2003**, *125*, 1532.
- Berti, P. J.; McCann, J. A. B. *Chem. Rev.* **2006**, *106*, 506.
- Sunko, D. E.; Szele, I.; Hehre, W. J. *J. Am. Chem. Soc.* **1977**, *99*, 5000.
- Sulzenbacher, G.; Driguez, H.; Henrissat, B.; Schulein, M.; Davies, G. J. *Biochemistry* **1996**, *35*, 15280.
- Vasella, A.; Davies, G. J.; Böhm, M. *Curr. Opin. Chem. Biol.* **2002**, *6*, 619.
- Schramm, V. L. *Annu. Rev. Biochem.* **1998**, *67*, 693.
- Dewar, M. J. S.; Zoebisch, E. G.; Healy, E. F.; Stewart, J. J. P. *J. Am. Chem. Soc.* **1985**, *107*, 3902.
- Stewart, J. J. P. *J. Comput. Chem.* **1989**, *10*, 209.
- McNamara, J. P.; Muslim, A.; Abdel-Aal, H.; Wang, H.; Mohr, M.; Hillier, I. H.; Bryce, R. A. *Chem. Phys. Lett.* **2004**, *394*, 429.
- Cui, Q.; Elstner, M.; Kaxiras, E.; Frauenheim, T.; Karplus, M. *J. Phys. Chem. B* **2001**, *105*, 569.
- Dixon, H. B. F. *Eur. J. Biochem.* **1980**, *111*, 295–298.
- Cremer, D.; Pople, J. A. *J. Am. Chem. Soc.* **1975**, *96*, 1354.
- Hill, A. D.; Reilly, P. J. *J. Chem. Inf. Model.* **2007**, *47*, 1031.
- Berces, A.; Enright, G.; Nukada, T.; Whitfield, D. M. *J. Am. Chem. Soc.* **2001**, *123*, 5460.
- Strümpfer, J.; Naidoo, K. *J. J. Comput. Chem.* **2010**, *31*, 308.
- Barnett, C. B.; Naidoo, K. *J. AIP Conf. Proc.* **2009**, *1102*, 214.
- Barnett, C. B.; Naidoo, K. *J. Mol. Phys.* **2009**, *107*, 1243.
- Brooks, B. R.; Brooks, C. L.; Mackerell, A. D.; Nilsson, L.; Petrella, R. J.; Roux, B.; Won, Y.; Archontis, G.; Bartels, C.; Boresch, S.; Caflisch, A.; Caves, L.; Cui, Q.; Dinner, A. R.; Feig, M.; Fischer, S.; Gao, J.; Hodoscek, M.; Im, W.; Kuczera, K.; Lazaridis, T.; Ma, J.; Ovchinnikov, V.; Paci, E.; Pastor, R. W.; Post, C. B.; Pu, J. Z.; Schaefer, M.; Tidor, B.; Venable, R. M.; Woodcock, H. L.; Wu, X.; Yang, W.; York, D. M.; Karplus, M. *J. Comput. Chem.* **2009**, *30*, 1545.
- Naidoo, K. J.; Brady, J. W. *J. Am. Chem. Soc.* **1999**, *121*, 2244.
- Rajamani, R.; Naidoo, K. J.; Gao, J. *J. Comput. Chem.* **2003**, *24*, 1775.
- Kumar, S.; Payne, P. W.; Vásquez, M. *J. Comput. Chem.* **1996**, *17*, 1269.
- Kumar, S.; Rosenberg, J. M.; Bouzida, D.; Swendsen, R. H.; Kollman, P. A. *J. Comput. Chem.* **1995**, *16*, 1339.
- Kumar, S.; Bouzida, D.; Swendsen, R. H.; Kollman, P. A.; Rosenberg, J. M. *J. Comput. Chem.* **1992**, *13*, 1011.
- Byun, K.; Mo, Y.; Gao, J. *J. Am. Chem. Soc.* **2001**, *123*, 3974.
- Pereira da Silva, C.; Araujo de Souza, A. *Quim. Brasil* **2007**, *1*, 57.
- Rungrotnongkol, T.; Mulholland, A. J.; Hannongbua, S. *J. Mol. Graphics Modell.* **2007**, *26*, 1.
- Zhou, H.; Tajkhorshid, E.; Frauenheim, T.; Suhai, S.; Elstner, M. *Chem. Phys.* **2002**, *277*, 91.
- Barnett, C. B.; Naidoo, K. *J. Phys. Chem. B* **2008**, *112*, 15450.

- (31) Woodcock, H. L.; Hodoscek, M.; Brooks, B. R. *J. Phys. Chem. B* **2007**, *111*, 20.
- (32) Xu, D.; Guo, H.; Cui, Q. *J. Am. Chem. Soc.* **2007**, *129*, 10814.
- (33) Appell, M.; Strati, G.; Willett, J. L.; Momany, F. A. *Carbohydr. Res.* **2004**, *339*, 537.
- (34) Steinmann, S. N.; Csonka, G.; Corminboeuf, C. *J. Chem. Theory Comput.* **2009**, *5*, 2950.
- (35) Csonka, G. I. *J. Mol. Struct.—Theochem* **2002**, *584*, 1.
- (36) Jalbout, A. F.; Adamowicz, L.; Ziurys, L. M. *Chem. Phys.* **2006**, *328*, 1.
- (37) Harvey, S. C.; Prabhakaran, M. *J. Am. Chem. Soc.* **1986**, *108*, 6128.
- (38) Bartels, C.; Karplus, M. *J. Comput. Chem.* **1997**, *18*, 1450.
- (39) Bartels, C.; Karplus, M. *J. Phys. Chem. B* **1998**, *102*, 865.
- (40) Ionescu, A. R.; Berces, A.; Zgierski, M. Z.; Whitfield, D. M.; Nukada, T. *J. Phys. Chem. A* **2005**, *109*, 8096.
- (41) Biarnes, X.; Ardevol, A.; Planas, A.; Rovira, A.; Laio, A.; Parrinello, M. *J. Am. Chem. Soc.* **2007**, *129*, 10686.
- (42) Segà, M.; Autieri, E.; Pederiva, F. *J. Chem. Phys.* **2009**, *130*.
- (43) Kurihara, Y.; Ueda, K. *Carbohydr. Res.* **2009**, *344*, 2266.
- (44) Davies, G. J.; Ducros, V. M. A.; Varrot, A.; Zechel, D. L. *Biochem. Soc. Trans.* **2003**, *31*, 523.
- (45) Ducros, V. M. A.; Zechel, D. L.; Murshudov, G. N.; Gilbert, H. J.; Szabó, L.; Stoll, D.; Withers, S. G.; Davies, G. J. *Angew. Chem.* **2002**, *114*, 2948.
- (46) Sabini, E.; Sulzenbacher, G.; Dauter, M.; Dauter, Z.; Jorgensen, P. L.; Schulein, M.; Dupont, C.; Davies, G. J.; Wilson, K. S. *Chem. Biol.* **1999**, *6*, 483.
- (47) Sidhu, G.; Withers, S. G.; Nguyen, N. T.; McIntosh, L. P.; Ziser, L.; Brayer, G. D. *Biochemistry* **1999**, *38*, 5346.

JP107620H